the plant journal

SEB SOCIETY FOR EXPERIMENTAL BIOLOGY

The Plant Journal (2020) **103,** 308–322 doi: 10.1111/tpj.14732

ZEITLUPE facilitates the rhythmic movements of *Nicotiana attenuata* flowers

Lucas Cortés Llorca[1], Ran Li[1,†], Felipe Yon[1,‡], Martin Schäfer[1,§], Rayko Halitschke[1], Christelle A.M. Robert[2,¶], Sang-Gyu Kim[1,‖] and Ian T. Baldwin[1]*

[1]*Department of Molecular Ecology, Max Planck Institute for Chemical Ecology, Jena, 007745, Germany, and*
[2]*Department of Biochemistry, Max Planck Institute for Chemical Ecology, Jena, 007745, Germany*

Received 30 October 2019; revised 31 January 2020; accepted 24 February 2020; published online 4 March 2020.
*For correspondence (e-mail baldwin@ice.mpg.de).
[†]Present address: State Key Laboratory of Rice Biology, Institute of Insect Sciences, Zhejiang University, Hangzhou, 310058, China
[‡]Present address: Centro de Innovación y Emprendimiento, Universidad Peruana Cayetano Heredia, Lima, 15102, Peru
[§]Present address: Institute for Evolution and Biodiversity, University of Münster, Münster, 48149, Germany
[¶]Present address: Institute of Plant Sciences, University of Bern, Bern, 3012, Switzerland
[‖]Present address: Department of Biological Sciences, Korea Advanced Institute of Science and Technology, Daejeon, 34141, South Korea

SUMMARY

Circadian organ movements are ubiquitous in plants. These rhythmic outputs are thought to be regulated by the circadian clock and auxin signalling, but the underlying mechanisms have not been clarified. Flowers of *Nicotiana attenuata* change their orientation during the daytime through a 140° arc to balance the need for pollinators and the protection of their reproductive organs. This rhythmic trait is under the control of the circadian clock and results from bending and re-straightening movements of the pedicel, stems that connect flowers to the inflorescence. Using an *explant* system that allowed pedicel growth and curvature responses to be characterized with high spatial and temporal resolution, we demonstrated that this movement is organ autonomous and mediated by auxin. Changes in the growth curvature of the pedicel are accompanied by an auxin gradient and dorsiventral asymmetry in auxin-dependent transcriptional responses; application of auxin transport inhibitors influenced the normal movements of this organ. Silencing the expression of the circadian clock component ZEITLUPE (ZTL) arrested changes in the growth curvature of the pedicel and altered auxin signalling and responses. IAA19-like, an Aux/IAA transcriptional repressor that is circadian regulated and differentially expressed between opposite tissues of the pedicel, and therefore possibly involved in the regulation of changes in organ curvature, physically interacted with ZTL. Together, these results are consistent with a direct link between the circadian clock and the auxin signalling pathway in the regulation of this rhythmic floral movement.

Keywords: ***Nicotiana attenuata*, plant movement, auxin signalling, circadian clock.**

INTRODUCTION

The study of plant movements has revolutionized the concept of plants as organisms capable of responding to their environment and has contributed to the discovery of fundamental biological processes such as the existence of endogenous rhythms and the growth hormone auxin (de Mairan, 1729; Darwin, 1880; Went, 1928). Circadian movements were first documented in the 18th century (de Mairan, 1729). Since then, a wide range of organ movements such as the ubiquitous circumnutation of stems, helical movement of elongating organs whose study was pioneered by Charles Darwin and his son, the opening and closing of flowers and changes in leaf and flower orientation, have been shown to be under the control of the circadian clock (Engelmann *et al.*, 1992; Niinuma *et al.*, 2005; Atamian *et al.*, 2016; Yon *et al.*, 2016).

At its simplest, the plant circadian clock encompasses over 20 transcription factors arranged in multiple interconnected transcriptional and translational feedback loops (Shalit-Kaneh *et al.*, 2018). The MYB transcription factors *LATE ELONGATED HYPOCOTYL* (*LHY*) and *CIRCADIAN CLOCK ASSOCIATED 1* (*CCA1*) are morning-expressed genes that repress the transcription of other clock components during the day (Adams *et al.*, 2015). As LHY and CCA1 protein levels decline, the mRNA levels of *PSEUDO RESPONSE REGULATORs* (*PRR*s) sequentially start to rise and, when translated into proteins, suppress the expression of LHY and CCA1 (Nakamichi *et al.*, 2010). At the end

of the day, GIGANTEA (GI), a plant-specific nuclear protein, stabilizes the F-box protein and blue-light photoreceptor ZEITLUPE (ZTL) which targets PSEUDO RESPONSE REGULATOR 1/TIMING OF CAB EXPRESSION 1 (PRR1/TOC1) for proteasome-dependent degradation (Más *et al.*, 2003; Kim *et al.*, 2007). At night, EARLY FLOWERING 3 (ELF3), ELF4 and the transcription factor LUX ARRHYTHMO (LUX) form a protein complex, known as the evening complex (EC), that represses the expression of PRRs (Helfer *et al.*, 2011; Tong *et al.*, 2020).

Functionally, circadian clock regulated movements have been associated with protection of vegetative and reproductive organs from abiotic factors, foraging for light and resources, temperature regulation and pollinator attraction (Atamian *et al.*, 2016; Yon *et al.*, 2017; Haverkamp *et al.*, 2018). Flowers of the wild tobacco *Nicotiana attenuata* change their orientation in a rhythmic manner through a 140° arc (Yon *et al.*, 2016). Functionally, the downwards orientation of flowers during the day helps to protect their reproductive organs from environmental factors (Haverkamp *et al.*, 2018). At night, when the plant's main pollinators *Manduca sexta* moths are active, the flowers' upwards orientation facilitates access of naive moths to flowers, enhancing pollination success (Yon *et al.*, 2017). Silencing the expression of the clock components LHY and ZTL alters this rhythmic behaviour. The period of the movement is significantly shorter in inverted-repeat stably transformed LHY (ir*LHY*) plants, whereas in *irZTL* this floral movement is almost completely abolished (Yon *et al.*, 2016). Similarly, the genetic manipulation of clock genes influences circadian movements such as the rhythmic leaf movements and circumnutation of inflorescence stems in Arabidopsis (Millar *et al.*, 1995; Niinuma *et al.*, 2005). Yet, the molecular mechanisms by which the circadian clock regulates these rhythmic outputs are still poorly understood.

Plant movements are driven by unequal rates of irreversible cellular growth, reversible changes in cell volume or a combination of both responses between opposite tissues of an organ. The hormone auxin has long been recognized as a central component in the regulation of growth responses in plants (Went, 1928). Auxin acts as a permissive signal for growth, providing cells the necessary competence to enter into the cell cycle through the regulation of CDK-inhibitory proteins (Himanen *et al.*, 2002). Auxin responsive elements (AuxREs) are present in the promoter regions of various cyclins and some of these genes are transcriptionally regulated by auxin (Roudier *et al.*, 2003; Ishida *et al.*, 2010). In addition, auxin promotes cell expansion by regulating the extensibility of the cell wall (Nishitani and Masuda, 1981; Kutschera and Schopfer, 1986). In directional growth movements (tropisms), asymmetry in auxin contents, and auxin-dependent transcriptional responses mediate the differences in elongation rates in stems, hypocotyls and roots that result in changes in growth curvature and the bending responses of these organs (Went, 1928; Briggs *et al.*, 1957; Li *et al.*, 1991; Tatematsu *et al.*, 2004; Esmon *et al.*, 2006). In Arabidopsis, auxin-dependent transcription during tropism involves a feedback loop mechanism with the activator AUXIN RESPONSE FACTOR 7 (ARF7) and the repressor INDOLE-3-ACETIC ACID INDUCIBLE 19 (IAA19), and mutants in these genes display altered tropic responses (Harper *et al.*, 2000; Tatematsu *et al.*, 2004). Similarly, an *IAA19*-like gene has been implicated in the regulation of the circadian clock-controlled heliotropic movements of sunflower heads due to its asymmetric expression between east and west sides of the stem (Atamian *et al.*, 2016). In Arabidopsis, the auxin-resistant *axr2-1* mutant abolishes both shoot circumnutational movements and tropic responses (Hatakeda *et al.*, 2003; Sato *et al.*, 2014), which further supports a role for auxin in the regulation of different types of growth movements. The circadian clock and auxin signalling also intersect in the tropic responses of potato and sunflower stems, where changes in the growth curvature in response to a directional stimulus are time-of-day dependent (Vinterhalter *et al.*, 2014; Atamian *et al.*, 2016). Moreover, core components of the auxin signalling machinery such as Aux/indole-3-acetic acids (IAAs), ARFs and the Myb-like transcription factor REVEILLE1 (REV1), which promotes the expression of the auxin biosynthetic gene *YUCCA8*, are under circadian control (Covington and Harmer, 2007; Rawat *et al.*, 2009).

The identification of clock-controlled effectors of differential growth responses could provide valuable insights into the mechanisms of regulation of circadian movements. Here, we address this question by investigating the molecular basis of the daily changes in orientation of *N. attenuata* flowers, a circadian-regulated movement that results from changes in the growth curvature of the pedicel. To analyze this organ-level behaviour, we used kinetic measurements of pedicel elongation and organ curvature using an explant system that captures all of the movement characteristics of the intact system, temporally and spatially resolved transcriptomics, and direct auxin measurements in pedicels of wild-type (WT) and plants silenced in the expression of the circadian clock component ZTL. We report that both the circadian clock and the auxin signalling pathway facilitate this rhythmic behaviour and provide evidence that supports a central role of ZTL in the regulation of differential growth responses in this circadian movement.

RESULTS

Changes in flower orientation are associated with asymmetric transcriptional responses between opposite tissues of the pedicel

The bending and re-straightening movements of the pedicel make flowers of *N. attenuata* change their orientation

(Figure 1a and Movie S1). Tissue-specific expression analysis in opposite sides of moving organs has been used to identify genes implicated in the regulation of differential growth responses during tropisms (Li *et al.*, 1991; Esmon *et al.*, 2006). To investigate the molecular basis of pedicel movements, we analyzed the transcriptomes of adaxial and abaxial tissues of this organ during the movement cycle using whole-genome microarrays. Pedicels of WT plants were collected at different times of the day corresponding to three distinct phases of the movement: before the initiation of the movement when pedicels were straight (Zeitgeber time 0, ZT0), at the time of maximum organ curvature (ZT6), and when pedicels returned to a straight position (ZT14). At each time point, pedicels were longitudinally bisected from the abscission zone (Az) to the base of the nectary (Nc) to separate adaxial (dorsal) and abaxial (ventral) tissues (Figure 1b). To resolve molecular profiles associated with differential growth responses in this organ, we analyzed the transcriptome of adaxial/abaxial tissues using a Bayesian approach (Aryee *et al.*, 2009). This analysis identified 361 genes with dorsiventral expression asymmetry in the pedicel throughout the movement cycle (*P*-value < 0.01, fold change >4; Data S1). To explore the molecular differences between adaxial and abaxial tissues, we used hierarchical clustering (HCL) analysis. This analysis discriminated six main gene clusters based on the spatial and temporal profiles of these genes (Figure 1c).

To obtain functional insights into these clusters, we performed gene ontology (GO) analyses. Among the six clusters, only clusters II, IV and VI had significantly enriched GO terms (Bonferroni, $P_{adj} < 0.05$). Cluster I encompassed genes upregulated in the abaxial side of the pedicel when flowers move to a downwards orientation (ZT0–ZT6). Small numbers of auxin- and gibberellin-related genes for example *Aux/IAA* transcriptional repressors, *EXPANSINs* and the growth regulating factor *PACLOBUTRAZOL RESISTANCE5 (PRE5)* were present in this cluster (Figure S1 and Data S1). Clusters II and III encompassed genes that were upregulated in the adaxial side at the time of maximum pedicel curvature (Figure 1d), when flowers are facing downwards (ZT6), albeit with differences in the expression at ZT14 when genes in cluster III were upregulated in the abaxial tissue (Figure S1). These clusters encompassed genes associated with the GO term xyloglucan metabolic process for example *XYLOGLUCAN ENDOTRANSGLUCOSYLASES/HYDROLASES* (*XTHs*) and *XYLOGLUCAN GALACTOSYLTRANSFERASE 2 (XLT2)* (Figure 1d) and genes involved in gibberellin metabolism such as a *GA20-oxidase* (*GA20ox*) (Figure S1). Genes in cluster IV were largely upregulated in the abaxial side of the pedicel at the time of maximum pedicel curvature when flowers are facing downwards (ZT6) (Figure 1e). This cluster encompassed a large number of genes with GO terms associated with the regulation of organ growth and auxin responses such as *Aux/IAAs*, *EXPs* and *SMALL-AUXIN UPREGULATED RNAs* (*SAURs*). Cluster V encompassed genes that were constitutively upregulated in the adaxial side of the pedicel and included, among others, three transcription factors belonging to the plant-specific TEOSINTE BRANCHED 1, CYCLOIDEA, PCF1 (TCP) family (Figure S1). Genes in cluster VI were upregulated in the adaxial side of the pedicel at the time of maximum organ curvature (ZT6) (Figure 1f). This cluster was enriched in GO terms associated with cell wall remodelling processes for example *XTHs*, *PECTINMETHYLESTERASE/PECTINESTERASE INHIBITORs* (*PMEs*) and *POLYGALACTURONASE13* (*PGL13*). Collectively, these results indicated that transcriptional responses associated with differential growth in the pedicel are dominated by genes involved in cell wall remodelling processes and the auxin signalling pathway.

An auxin gradient between adaxial/abaxial tissues is established and maintained during pedicel movements

The formation of an auxin gradient is central to growth movements in different organs. Indole-3-acetic acid (IAA) levels were significantly higher at the time of maximum pedicel curvature (ZT6) (Figure 2a). Therefore, we measured IAA in adaxial and abaxial tissues during the movement cycle. IAA contents did not differ between these tissues before the initiation of the movement, when pedicels were straight (ZT0) (Figure 2b). However, at the time points when pedicels are bending (ZT2–ZT6) and re-straightening (ZT6–ZT10), significantly higher levels of IAA accumulated in the abaxial side (ratio *c.* 2:1), a result that is consistent with the upregulation of auxin-related genes in this tissue at ZT6 (Figure 1e). At the final phase of the movement, when pedicels had returned to straight positions (ZT14), IAA contents did not differ between adaxial and abaxial tissues.

Pedicel movements are organ autonomous and are dependent on auxin transport

Growth and curvature measurements in moving organs *in planta* are challenging and require specialized set-ups that frequently limit their spatial and temporal resolution. In addition, some plant movements result from the combination of growth and curvature responses of different organs or parts of an organ (Barlow, 1989; Dornbusch *et al.*, 2014). These limitations challenge mechanistic interpretations of data, as the spatial integrity of the responses is frequently lost during the movement. To overcome these limitations, we used an explant system that allowed us to explore pedicel growth and curvature responses with high spatial and temporal resolution. Pedicels of WT plants growing under long day (LD) conditions were collected before the initiation of the movement (ZT0) and incubated *in vitro* under a light intensity of 150 μmol m^{-2} sec^{-1}. Excised organs were recorded for one full cycle of the movement using time-

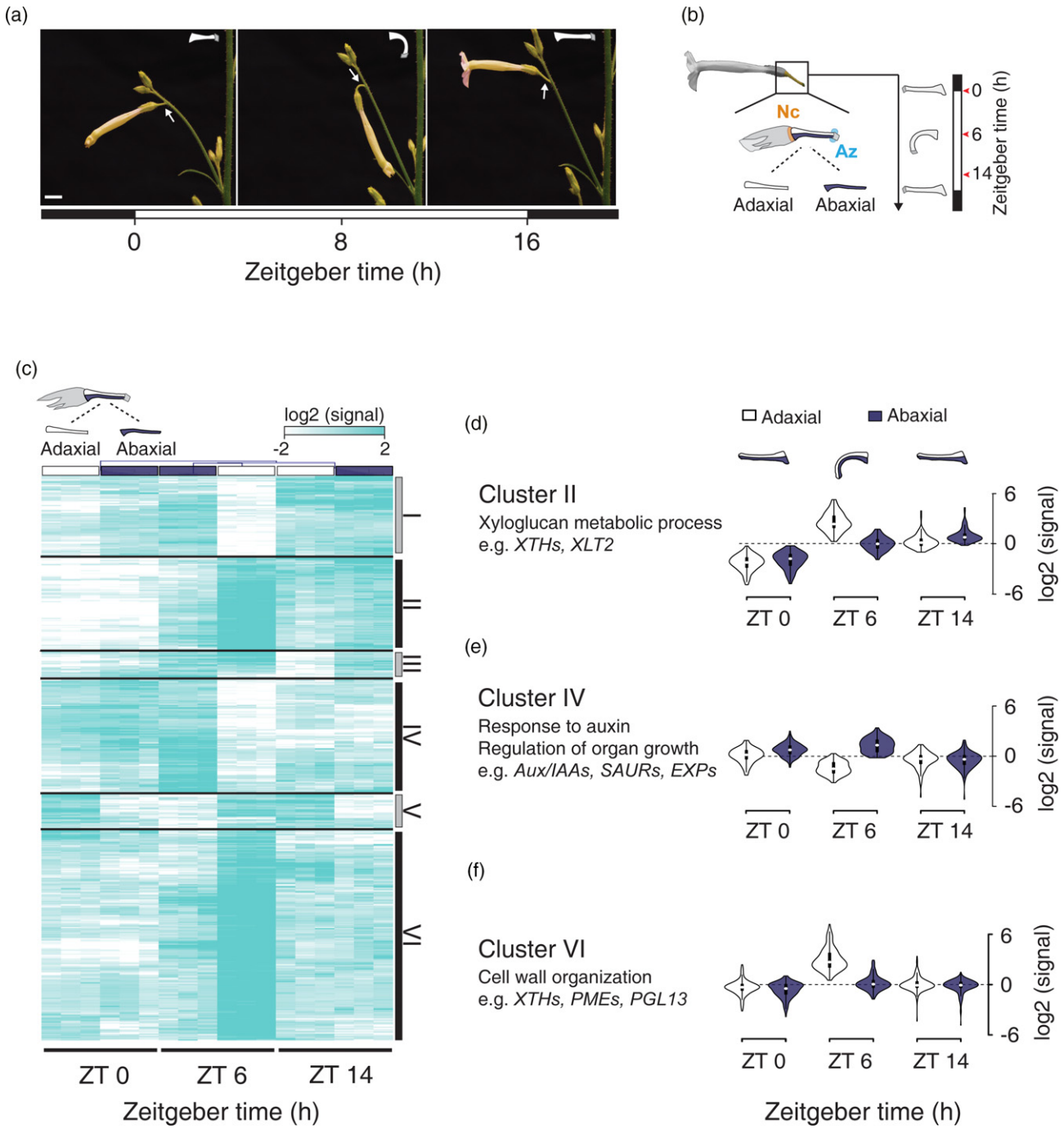

Figure 1. Changes in flower orientation are associated with asymmetric transcriptional responses between adaxial/abaxial tissues of the pedicel.
(a) Diurnal changes in flower orientation in *Nicotiana attenuata*. Flowers change their orientation through a 140° arc by sequentially bending and straightening their pedicels over 16 h during the light period. Pedicels of upwards facing flowers bend during the first phase of the movement (ZT0–ZT8). At the second phase of the movement (ZT8–ZT16), bent pedicels return to straight positions allowing flowers to face upwards at night when their corollas normally open, release scents and pollen, and are pollinated by nocturnal hawkmoth pollinators. Representative images of changes in pedicel size and curvature at different times throughout the movement cycle are indicated in the upper right corner. Arrows indicate the floral pedicel (see also Movie S1). Bar, 10 mm.
(b) Experimental design: pedicels were collected at the indicated times of the day (red arrowheads) and longitudinally bisected from the abscission zone (Az) to the base of the nectary (Nc) to separate adaxial from abaxial tissues.
(c) Hierarchical clustering of microarray probes with significant differences in signal intensity between adaxial and abaxial tissues of the pedicel throughout the movement (BETR, *P*-value < 0.01, fold change >4; see also Figure S1 and Data S1). Clusters with significant GO terms are indicated with a black box adjacent to the cluster number (Bonferroni, $P_{adj} < 0.05$).
(d–f) Violin plots showing the signal intensity of probes in (d) cluster II, (e) cluster IV and (f) cluster VI. Main gene ontology (GO) terms and genes associated with each cluster are highlighted.

lapse photography (Figure 3a). Pedicel movements in this *explant* system mimicked *in planta* responses, namely bending and re-straightening, as indicated by changes in organ curvature (Figure 3b and Movie S2). We found that pedicels continuously elongate during the movement cycle (Figure 3b) and the initiation of changes in organ curvature occurs *c.* 2 h after the night-day transition (ZT2) (Figure 3b, inset).

To gain further insights into the role of auxin in the growth curvature responses of the pedicel, we conducted experiments with intact plants using pedicel-targeted applications of the auxin efflux inhibitor 2,3,5-triiodobenzoic acid (TIBA). Lanolin mixtures with TIBA or DMSO (mock) were applied to pedicels of flowers of WT plants before lights off at ZT16 on the day before anthesis. Measurements were taken 8 h later at ZT0 for a period of 16 h. Flower position was recorded using a time-lapse imaging set-up and flower angle was measured with reference to the horizontal axis (Yon *et al.*, 2016). The TIBA treatment arrested flower reorientation (upwards movement), as indicated by significant differences in the flower angle at the end of the movement cycle (Figure 3c). We next tested the effect of exogenous applications of IAA and the auxin efflux inhibitor naphthylphthalamic acid (NPA) at distinct phases of the movement using the explant system. IAA addition to the incubation medium influenced organ curvature (Figure 3d) and promoted pedicel elongation (Figure 3e) irrespective of the time of the treatment. NPA treatment at the bending phase of the movement (ZT0–ZT4) influenced neither organ curvature nor pedicel elongation (Figure 3d,e), whereas the same treatment at the re-straightening phase (ZT8–ZT12) significantly altered organ curvature (Figure 3d), albeit without affecting organ elongation (Figure 3e). These results were consistent with the results *in planta*, namely the application of an auxin efflux inhibitor blocks pedicel re-straightening, but not the initial organ bending.

ZEITLUPE is necessary for normal growth movements of the pedicel and the expression of genes with dorsiventral asymmetry

We previously reported that silencing the circadian clock component ZTL arrested the diurnal changes in flower orientation of *N. attenuata* flowers (Yon *et al.*, 2016). To determine the function of ZTL in pedicel movements, we measured organ length and curvature kinetics in the empty vector (EV) and two independent ir*ZTL* lines throughout the movement cycle in the *explant* system. We found that pedicel curvature was significantly reduced in ir*ZTL* lines compared with the EV controls (Figure 4a). Similarly, increments in pedicel length during the movement cycle were strongly reduced in ir*ZTL* plants (Figure 4b). To capture the early molecular events leading to differences in the development of the initial organ curvature, we analyzed the transcriptome of EV and ir*ZTL* pedicels using whole-genome microarrays. This analysis identified 182 differentially expressed genes (DEGs) in ir*ZTL* pedicels relative to the EV controls at ZT0, before differences in organ curvature between genotypes became apparent (moderated *t*-test, $P_{adj} < 0.05$, fold change >2; Data S2). This set of genes encompassed the circadian clock components *LHY*, *LUX*, *ELF4*-like and the circadian-regulated *CHLOROPHYLL A/B-BINDING* (*CAB*) genes (Data S2), which is consistent with a function of ZTL in the regulation of circadian rhythms in the pedicel. Comparison of DEGs in ir*ZTL* pedicels at ZT0 with genes showing dorsiventral expression asymmetry in at least one time point during the movement cycle in WT plants (Data S1), and therefore possibly involved in the regulation of the growth movements of the pedicel, revealed 12 genes common to these two groups (Figure 4c). This set of genes encompassed two auxin-related genes: the auxin transcriptional repressor *IAA19*-like and a *SAUR* gene (*AX10A*) (Figure 4c).

The Aux/IAA transcriptional repressor IAA19-like is under the control of the circadian clock

Because Aux/IAAs are core components of the auxin signalling machinery and have been previously associated with other circadian and directional growth movements (Tatematsu *et al.*, 2004; Atamian *et al.*, 2016), we analyzed the expression levels of *IAA19*-like throughout the movement cycle in pedicels of EV and ir*ZTL* plants. *IAA19*-like was largely downregulated in ir*ZTL* at the times when EV pedicels were bending ZT0–ZT4 (Figure 5a), which was consistent with microarray results and supported the role for this gene as positive regulator of changes in the growth curvature of the pedicel. IAA19-like belongs to the IAA5/6/19 clade of Aux/IAA genes, which are predominantly expressed in flowers as indicated by RNA-seq data of 13 different tissues (Figure S2a). The expression of *IAA19*-like is highest in the pedicel (Figure S2b) and its transcript levels are rapidly upregulated in response to exogenous auxin treatments, albeit the upregulation did not differ (fold change >2) between EV and ir*ZTL* pedicels at any of the assayed auxin concentrations (Figure S2c). Subcellular localization of IAA19-like–YFP fusion protein in *Agrobacterium*-infiltrated *N. benthamiana* leaf cells indicated that IAA19-like was localized in the nucleus (Figure S2d), consistent with nuclear localization of other Aux/IAA proteins (Abel *et al.*, 1994).

Direct auxin measurements in the pedicel revealed that IAA levels did not differ significantly between EV and ir*ZTL* lines at ZT0 (Figure 5b), indicating that additional factors contributed to the downregulation of *IAA19*-like in ir*ZTL* pedicels. Analysis of the transcript levels of *IAA19*-like in the leaves of early rosette-stage plants in diurnal (LD) conditions revealed that, similar to the response observed in pedicels, the transcript levels of *IAA19*-like were largely

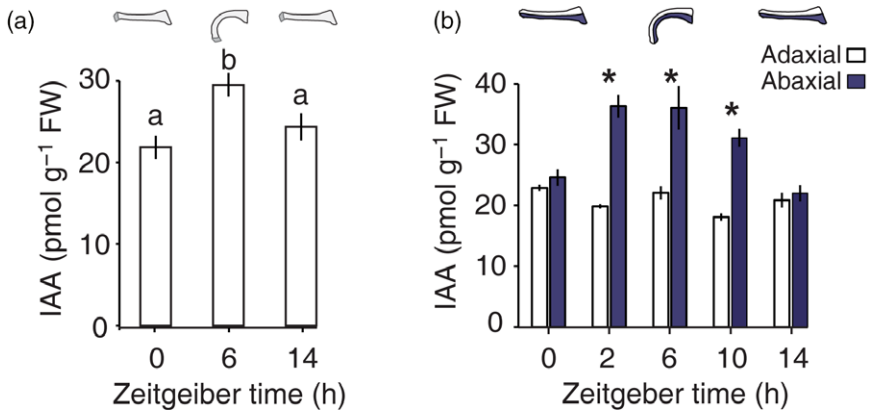

Figure 2. Spatial and temporal changes in auxin contents in the pedicel are consistent with a role for auxin in the control of growth curvature responses in this organ.
(a) Endogenous indole-3-acetic acid (IAA) contents in the entire pedicel at distinct phases of the movement (mean ± SEM, $n = 3$). [a,b]Different letters indicate significant differences among time points, as determined by ANOVA followed by Tukey's test ($P < 0.05$).
(b) Endogenous IAA contents in adaxial and abaxial tissues of the pedicel at distinct phases of the movement (mean ± SEM, $n = 3$). Asterisks indicate significant differences in IAA content between adaxial and abaxial tissues at the indicated time (Student's *t*-test, $P < 0.05$).

downregulated at ZT0 (Figure 5c). Furthermore, cycling of the mRNA levels of *IAA19*-like in EV under continuous light (LL) conditions (Figure 5c) indicated that this gene was under the control of the circadian clock. Because changes in the accumulation of Aux/IAA proteins could feed back on their own genes to regulate their expression and ZTL has been shown to directly regulate the stability of several proteins (Más *et al.*, 2003; Kiba *et al.*, 2007; Liu *et al.*, 2013; Li *et al.*, 2018), we investigated if ZTL and IAA19-like could physically interact. Analysis of tissue-specific and temporal expression patterns of *ZTL* and *IAA19*-like indicated that their proteins are likely to co-occur spatially and temporally in this organ (Figures S2 and S3). Therefore, we performed a yeast-two-hybrid assay using ZTL and IAA19-like as bait and prey, respectively. Yeast-two-hybrid results indicated that ZTL interacted with IAA19-like (Figure 5d), which was further confirmed with an *in vitro* pull-down assay with *E. coli* expressing GST–ZTL and His-IAA19-like (Figure 5e). In addition, an *in vivo* co-immunoprecipitation assay in *N. benthamiana* transiently overexpressing YFP–ZTL and IAA19-like-Myc revealed that IAA19-like effectively co-immunoprecipitated with ZTL (Figure 5f).

Silencing ZTL affects auxin responses in the pedicel in a time-of-day-dependent manner

We next investigated if auxin responses were altered in pedicels of ir*ZTL* plants. We measured pedicel elongation in response to exogenous applications of IAA and 2,4-dichlorophenoxyacetic acid (2,4-D), a synthetic auxin that is a poor substrate for IAA-conjugating enzymes and its transport does not depend on efflux carriers (Delbarre *et al.*, 1996; Staswick *et al.*, 2005). Pedicels were collected at ZT0, ZT8, and ZT16 and incubated in mock or auxin solutions. Organ elongation was measured 6 h after the initiation of each treatment at ZT0+6, ZT8+6, and ZT16+6. The increments in pedicel length in response to IAA and 2,4-D treatments initiated at ZT0 were significantly larger in ir*ZTL* compared with the EV controls (Figure 6a). In treatments initiated at ZT8, increments in pedicel length did not differ between EV and ir*ZTL* in the IAA and the 2,4-D treatments (Figure 6b). At ZT16, the increments in pedicel lengths in response to IAA were slightly, but significantly, larger in ir*ZTL* compared with the EV controls (Figure 6c), whereas no differences were observed in the 2,4-D treatment.

DISCUSSION

Circadian organ movements are widespread among plants. Yet, the molecular mechanisms underlying these movements are not fully understood. Previously, we showed that the circadian clock regulated daily changes in flower orientation in *N. attenuata* (Yon *et al.*, 2016). Here, we advance our mechanistic understanding of this movement and demonstrated that this rhythmic behaviour is under the control of the circadian clock and the auxin signalling pathway.

The results from this non-model system provide a new perspective into the transcriptional responses associated with differential growth in moving organs. This task has been challenging in hypocotyls and roots during tropisms, due to their small size, and in circumnutating stems where the axis of symmetry of the movement is continuously changing. To overcome these limitations, whole-genome microarrays designed from Arabidopsis were used to investigate the transcriptional responses during the movements of gravi-stimulated and photostimulated seedlings in its close relative *Brassica oleracea*, which has dramatically larger hypocotyls in comparison with those of

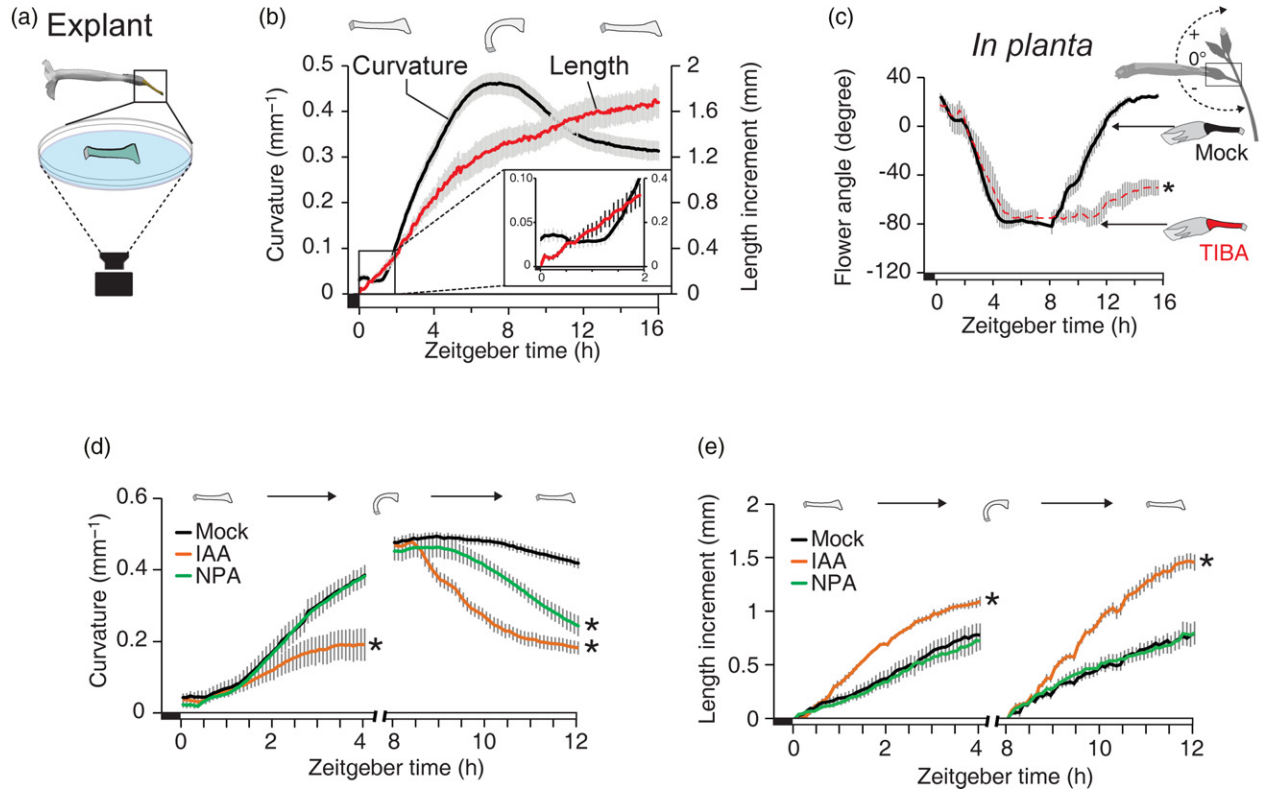

Figure 3. An explant system recapitulates the effect of blocking auxin transport *in planta*.
(a) Scheme of the experimental setup used for measuring pedicel curvature and elongation of explants *in vitro* (see also Movie S2).
(b) Length increment (red line) and curvature (black line) kinetics of pedicels from WT plants *in vitro* (mean ± SEM, $n = 11$). Pedicels were collected from plants growing under long day (LD) conditions at ZT0 and transferred to *in vitro* conditions under continuous white light. Excised pedicels were imaged every 5 min for 16 h for one full cycle of bending and re-straightening, as schematically indicated in the upper part of the panel. The figure inset shows pedicel length increments and curvatures from ZT0 to ZT2 which indicate that increment in pedicel length precedes changes in organ curvature.
(c) Pedicel-targeted application of the auxin transport inhibitor TIBA on intact plants arrests flower reorientation (mean ± SEM, $n = 3$–4). Lanolin mixtures with 1.5 mg g^{-1} of TIBA or DMSO (mock) were applied to pedicels of flowers of intact plants before lights off at ZT16. Flower angle measurements were taken for a period of 16 h starting 8 h after application of the TIBA treatment at ZT0 on the next day. Asterisk indicates significant differences between treatments at the end of the time series when flowers in the mock treatment return to an upwards orientation (Student's *t*-test, $P < 0.05$).
(d) Curvature and (e) length increments of pedicel explants treated with 10 μM IAA, 100 μM NPA, and DMSO (mock) at the bending and straightening phases of the movement (mean ± SEM, $n = 8$). Pedicels were collected from WT plants at ZT0 and ZT8 and incubated in the indicated treatment for 4 h. Asterisks indicate significant differences between the mock and the IAA and NPA treatments in pedicels collected at ZT0 and ZT8 at ZT4 and ZT12, respectively (ANOVA, $P < 0.05$).

Arabidopsis (Esmon *et al.*, 2006). Similar to the transcriptional responses reported during the tropic responses of *B. oleracea* seedlings, changes in the growth curvature of the pedicel in *N. attenuata* were accompanied by asymmetry in auxin-dependent transcriptional responses (Figure 1e). Notably, among these genes we found several *Aux/IAA*s with higher expression levels in the abaxial side of the pedicel. Asymmetrical expression of these core components of the auxin signalling machinery has been reported in the circadian-regulated heliotropic movements of sunflower heads and is essential for eliciting a normal tropic response in Arabidopsis (Li *et al.*, 1991; Esmon *et al.*, 2006; Taniguchi *et al.*, 2014). Together, these results further support a central role for Aux/IAAs in the regulation of the differential growth responses in different types of movements and organs. Adding to this picture, several gibberellin (GA)-related genes showed asymmetrical expression patterns in the pedicel (Figure S1, clusters I and III). Asymmetry in GA contents has been reported in the geotropic responses of roots, excised shoot tips and in the bending zone of circumnutating epicotyls (Phillips, 1972; Löfke *et al.*, 2013; Iida *et al.*, 2018). Interestingly, we found a large expression polarity in TCP transcription factors that were constitutively upregulated in the adaxial side of the pedicel (Cluster V; Figure S1), which has not been previously associated with any other type of growth movement.

Changes in flower orientation in *N. attenuata* are under the control of the circadian clock (Yon *et al.*, 2016). However, we did not find differences in the expression of circadian clock components between adaxial and abaxial tissues of the pedicel during the movement cycle (Data S1). This result is consistent with the lack of asymmetric

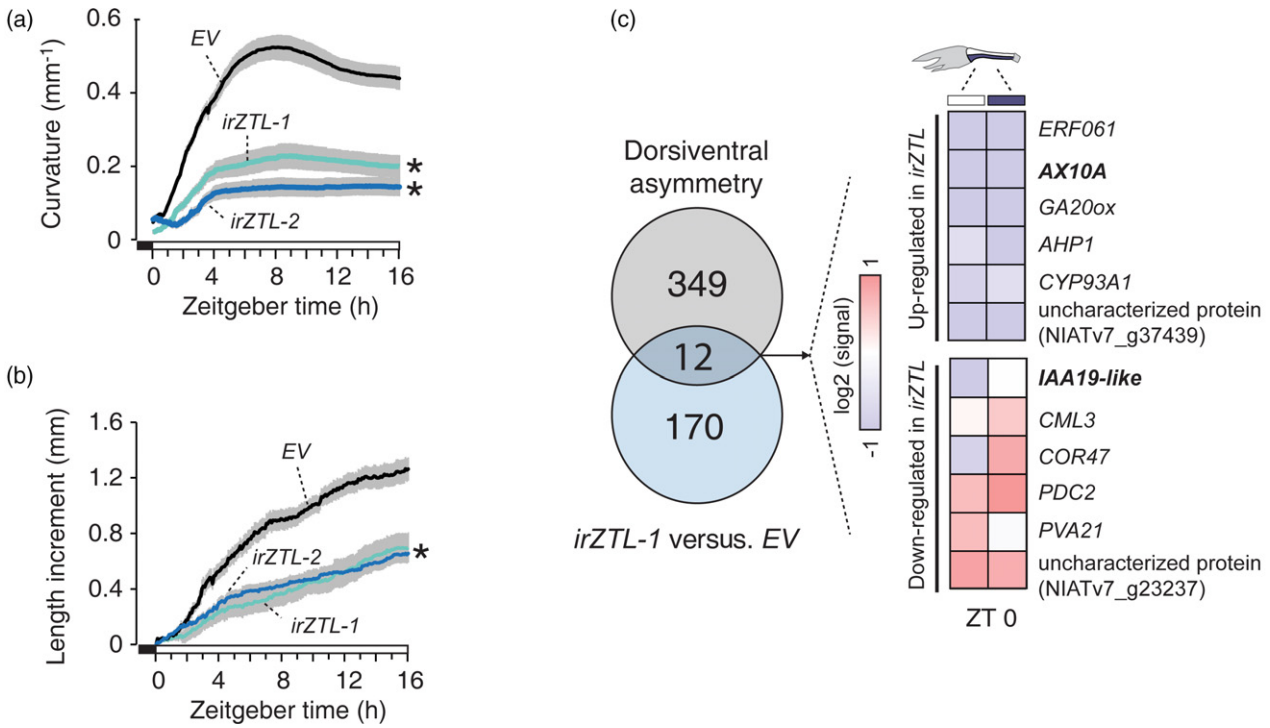

Figure 4. ZEITLUPE is necessary for the normal growth curvature responses and asymmetric gene expression in the pedicel.
(a) Curvature and (b) length increments in pedicels of EV and *irZTL* plants *in vitro* (mean ± SEM, $n = 11$). Asterisks indicate significant differences between EV and the two independent *irZTL* lines at ZT16 (ANOVA, $P < 0.05$).
(c) Venn diagram indicating the number of genes with dorsiventral expression asymmetry in opposite sides of pedicels of WT plants in at least one time point during the movement cycle (grey circle) and differentially expressed in *irZTL* pedicels relative to EV controls at ZT0 (blue circle) (moderated *t*-test, $P_{adj} < 0.05$, fold change >2; see also Data S2). The heatmap represents the expression of genes common to these two groups in adaxial/abaxial tissues at ZT0. Upregulated and downregulated genes in *irZTL* pedicels at ZT0 are indicated adjacent to the heatmap. Auxin related genes are highlighted.

expression of *TOC1*-like and *LHY*-like genes in opposite sides of stems in the circadian-regulated heliotropic movements of sunflower (Atamian *et al.*, 2016). Together, these results suggested that differential growth responses in rhythmic movements may not arise from differences in the circadian clock between opposite tissues of an organ. Therefore, it seems likely that the function of the clock in these movements is gating tissue-specific signals such as auxin.

In this work, we showed that, similar to other growth movements, changes in the growth curvature of the pedicel were associated with the establishment of an auxin gradient between adaxial/abaxial tissues at early stages of the movement cycle (Figure 2b), but the patterns differed from expectations. We found increased auxin accumulation in the abaxial side of the pedicel during both the bending and straightening phases of the movement, indicating that there was not a simple relationship between auxin distribution and changes in the growth curvature of this organ. In roots, increased auxin accumulation in bottom tissues in response to gravi-stimulation inhibited growth, leading to the downwards bending (Estelle, 1996) whereas, in hypocotyls, increased auxin accumulation in the side furthest from the incident stimuli had the opposite effect, namely promoting growth and leading to the subsequent curvature response (Esmon *et al.*, 2006). The patterns of auxin distribution and growth curvature responses in the pedicel resemble those of autotrophic responses of pea epicotyls (Haga and Iino, 2006), in which the side of the organ with the auxin maxima does not correlate with the expected direction of the growth curvature response for an aboveground organ. Thus, the auxin gradient and its effect on differential growth responses and the subsequent changes in curvature depended on the type of organ and movement. To date, no hormonal gradients have been reported for other circadian-regulated movement and it is possible that the patterns of auxin distribution in the pedicel and its relationship with changes in the growth curvature response are common in these types of movements. Moreover, the flower pedicel, with its stem-like structure, originates from a floral meristem, and separates it from previously studied growth movements in vegetative tissues such as roots, hypocotyl, stems, and coleoptiles. Analogous to the differences in auxin sensitivity between

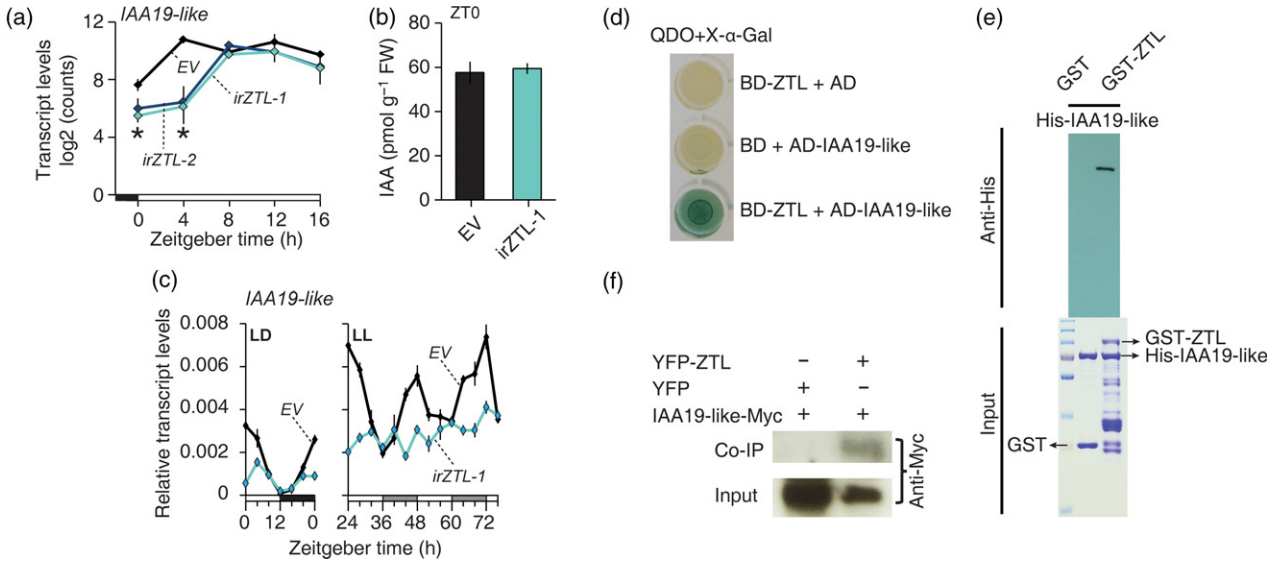

Figure 5. The transcriptional repressor IAA19-like is under circadian regulation.
(a) Transcript levels of *IAA19*-like in pedicels of EV and *irZTL* plants throughout the movement cycle (mean ± SD, $n = 3$). Asterisks indicate significant differences between EV and the two independent *irZTL* lines at the indicated times (ANOVA, $P < 0.05$, fold change >1.5).
(b) IAA quantification in pedicels of EV and *irZTL* plants at ZT0 (mean ± SEM, $n = 5$).
(c) Relative transcript levels of *IAA19*-like in leaves of early rosette-stage EV and *irZTL* plants under diurnal (LD) and continuous light conditions (LL) as determined by qPCR (mean ± SEM, $n = 4$–5). Plants were grown in a 12:12 h (light:dark) photoperiod before being transferred to LL conditions. Night and subjective night periods are indicated in the time axis with black or grey boxes, respectively. *EF1α* was used as reference gene.
(d) Yeast-two-hybrid assays of the interaction between ZTL and IAA19-like proteins. BD-ZTL and AD-IAA19-like were co-transformed into the yeast strain Y2H-gold. BD-ZTL+AD and BD+AD-IAA19-like co-transformed yeast were used as controls. Transformants were grown on QDO (SD -Ade/-His/-Leu/-Trp) plates with 40 mg L^{-1} of X-α-Gal.
(e) *In vitro* pull-down assays. GST–ZTL was used to pull down 2 μg of His-IAA19-like and immunoblotted by anti-His antibody. Proteins were visualized by Coomassie blue staining to monitor the protein input amounts.
(f) *In vivo* co-immunoprecipitation assays. Protein extracts of *Nicotiana benthamiana* leaves expressing YFP/IAA19-like-Myc or YFP–ZTL/IAA19-like-Myc were immunoprecipitated with GFP-Trap_A beads. Input proteins and immunoprecipitates were immunoblotted by anti-Myc antibody.

shoots and roots, it is conceivable that the particularities in auxin signalling in floral organs shape the auxin-mediated differential growth responses in the pedicel (Paponov *et al.*, 2008).

A marked characteristic of the pedicel is its capacity to sustain movement behaviour, even when excised (Movie S1 and Figure 3b). Bending and re-straightening of pedicel explants under *in vitro* conditions implied that the mechanisms regulating this movement were organ-autonomous. These must include hormone metabolism and other growth-related processes involved in differential growth. Along these lines, applications of the auxin efflux inhibitors TIBA and NPA (Morris *et al.*, 2010) did not influence curvature responses in the pedicel during the bending phase of the movement (Figure 3c,d), when auxin accumulated to higher levels in the abaxial tissue (Figure 2b), suggesting that the establishment of the auxin gradient in this organ could result from local changes in auxin metabolism: perhaps an increase in the rate of synthesis and/or degradation of auxin. While this proposed mechanism for the establishment of the auxin gradient differed substantially from that reported in tropic responses in coleoptiles and hypocotyls, which rely on auxin transport, it resembled that of grass nodes during geotropic bending in which the auxin gradient results from local changes in auxin metabolism rather than from an auxin redistribution process (Wright *et al.*, 1978). Adding to this picture, we found that TIBA and NPA applications effectively blocked pedicel re-straightening, indicating that auxin efflux is necessary during the second phase of the movement when flowers return to an upwards orientation.

The use of mutants in Arabidopsis has greatly advanced our mechanistic understanding of plant movements (Tatematsu *et al.*, 2004; Niinuma *et al.*, 2005). Here, we found that silencing the expression of the circadian clock component ZTL arrested the growth movements of the flower pedicel in the wild tobacco *N. attenuata* (Figure 4a). Similarly, circadian leaf movements, which are largely driven by variations in cell volume (Somers *et al.*, 2000), were abolished under red light conditions in *ztl* mutants in Arabidopsis (Jarillo *et al.*, 2001). Thus, ZTL acts as a positive regulator of circadian movements in different organs. We found that auxin responses were also altered in ir*ZTL* plants (Figure 6a). In Arabidopsis, growth phenotypes of

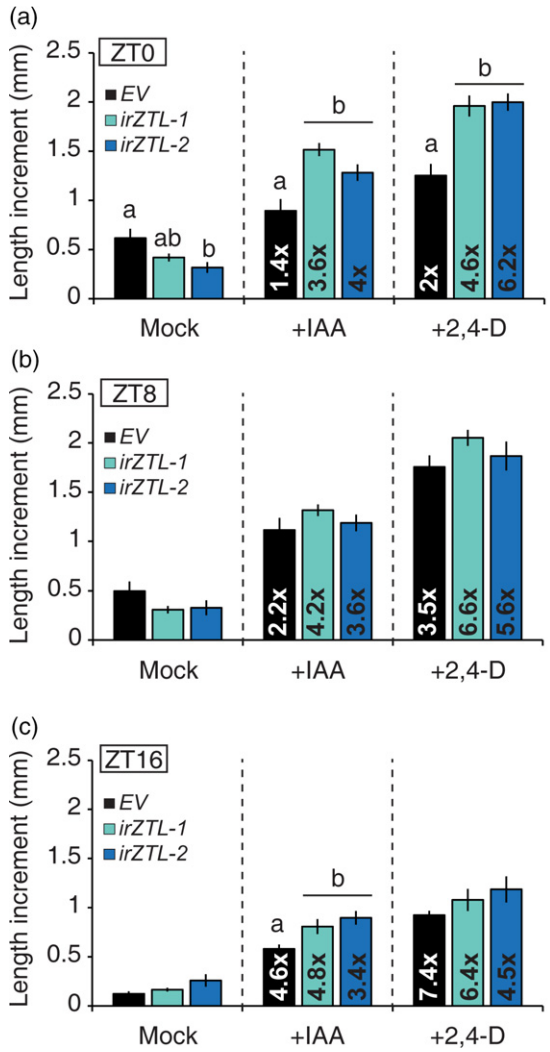

Figure 6. ZTL silencing affects pedicel elongation in response to exogenous auxin in a time-of-day dependent manner. Length increments in pedicels of EV and ir*ZTL* plants in response to exogenous IAA and the synthetic auxin 2,4-D in treatments initiated at different times of the day (mean ± SEM, $n = 5$–11). Pedicels were collected at ZT0, ZT8 and ZT16 and incubated in 10 μM IAA, 5 μM 2,4-D or mock solutions for 6 h. Increments in pedicel lengths were determined at (a) ZT0+6, (b) ZT8+6 and (c) ZT16+6. The ZT time at which treatments were initiated is indicated at the top of each panel. Fold induction in pedicel length relative to the respective mock is highlighted. [a,b]Different letters indicate significant differences among EV and ir*ZTL* lines in each treatment, as determined by ANOVA followed by Tukey's test ($P < 0.05$).

ztl mutants and ZTL overexpressors have been related to defects in auxin responses (Saitoh *et al.*, 2015a,b), pointing towards a general function of ZTL in the regulation of auxin-mediated growth responses. The increased pedicel elongation in ir*ZTL* at ZT0 in response to both exogenous IAA and 2,4-D treatments, suggests that neither auxin transport nor conjugation processes are involved in this differential response.

Notably, we found that the transcript levels of the Aux/IAA transcriptional repressor *IAA19*-like, a gene with asymmetrical expression in the pedicel, and therefore possibly involved in the regulation of differential growth responses in this organ, were strongly downregulated in ir*ZTL*, a result that is consistent with the downregulation of auxin-inducible genes in *ztl* mutants in Arabidopsis, for example Aux/IAAs and *SAUR*s (Saitoh *et al.*, 2015a). We found that transcript levels of *IAA19*-like were under the control of the circadian clock (Figure 5c) and that ZTL and IAA19-like proteins physically interacted (Figure 5d–f). Two central questions remain to be explored regarding the interaction between ZTL and Aux/IAA proteins: (i) Is the stability of Aux/IAAs affected by ZTL? and (ii) Does auxin stimulate binding of the ubiquitin ligase SCF^{ZTL} to Aux/IAAs? We previously reported that the stability of JAZb, a transcriptional repressor that binds and inactivates the transcription of jasmonate (JA) responsive genes, is partly ZTL dependent and is not influenced by the active form of the jasmonate hormone jasmonoyl-L isoleucine (JA-Ile) (Li *et al.*, 2018). Mechanistic similarities between auxin and JA signalling pathways (Cuéllar Pérez and Goossens, 2013), suggested that ZTL could have a similar function in regulation of the stability of Aux/IAAs. However, further characterization of the interaction between Aux/IAAs and ZTL proteins will be necessary to support this hypothesis.

The extensive study of tropisms has revealed some important principles of growth movements in plants such as the site and mechanisms of perception of the external stimuli, establishment of the auxin gradient, and differential growth responses and subsequent change in organ curvature (Briggs, 2014). However, a wide range of organ movements still remains to be explored. A full understanding of the mechanisms underlying plant movements will require their study in non-model organisms and in different types of organs. Flowers present a great variety of growth movements in almost all floral parts, for example pistil (style), stamen (filament), pedicels, and corolla (petals) (Ruan and da Silva, 2011; Yon *et al.*, 2016). These movements are particularly worthy of additional mechanistic studies given their determinate developmental programmes and their function in mediating the sexual behaviour of plants. Here, we have laid the groundwork for deciphering the molecular basis of the growth movements of the pedicel, the organ responsible for the circadian changes in orientation of *N. attenuata* flowers. Our results demonstrated that this movement is organ autonomous and is mediated by the plant hormone auxin. We have shown that changes in the growth curvature of the pedicel are accompanied by lateral auxin gradients and dorsiventral asymmetry in auxin-dependent transcriptional responses, and applications of auxin transport inhibitors alter this movement. By silencing ZTL expression, we

demonstrated that this circadian clock component was necessary for normal pedicel movements and auxin signalling and responses in this organ. Moreover, we provided evidence that supports that the regulation of core components in the auxin signalling machinery by the circadian clock, at transcriptional and post-translational level, facilitates rhythmic changes in orientation of flowers in this wild tobacco species. In summary, this new system provides novel insights into the molecular mechanisms underlying a circadian-regulated floral trait and opens potential avenues to explore the relationship among different types of movements in plants (Darwin, 1880; Firn and Myers, 1989).

EXPERIMENTAL PROCEDURES

Plant material and growth conditions

Seeds of the 31st generation of the inbred 'UT' line of *N. attenuata* were used as WT plants. The previously described homozygous RNAi lines were all produced by transforming the WT genotype using the *Agrobacterium tumefaciens*-mediated procedure described in Krügel *et al.* (2002) and are the second and third generations of *irZTL-314* (*irZTL-1*), *irZTL-318* (*irZTL-2*) (Yon *et al.*, 2016) and the empty vector control EV-*266*. Seed germination procedure and glasshouse growth conditions were as described previously (Krügel *et al.*, 2002; Schuman *et al.*, 2014). Plants used for circadian time series were grown in a climate chamber under a 12:12 h (light:dark) photoperiod before transferring to continuous light conditions.

Pedicel length and curvature measurements

Pedicels were excised from donor plants at the indicated times and incubated in 10^{-3} M phosphate buffer pH 6.3 as described in Rayle *et al.* (1970) with 0.03% plant agar (Duchefa; https://www.duchefa-biochemie.com) under a light intensity of 150 μmol m^{-2} sec^{-1}. Pedicels were imaged using backlight illumination every 5–10 min with a Canon EOS Rebel T3 camera activated by a remote timer controller (Phottix TR- 90; http://www.phottix.com). Image sequences were converted to video using ImageJ software (Schneider *et al.*, 2012) and imported into the video analysis and modelling tool TRACKER v4.93 (available at https://physlets.org/tracker/) for analysis. Three points at the base, centre and apex of the pedicels were tracked in every frame of the video and a circle was fitted across the midline of the pedicel. The angle between the centre of the circumference and the basal and apical points of the pedicel was measured with the protractor tool. Curvature was calculated as the inverse of the radius of the circumference. Length was determined using the arc length formula ($s = r\theta$) where s represents the pedicel length, r is the radius of the circumference and θ is the angle in radians between the centre of the circumference and the apical and basal points of the pedicel. Pedicels that were not horizontally placed or overlapped in the images were excluded from analysis.

Flower angle measurements

Flower position was recorded using a time-lapse imaging setup and pictures were analyzed using the software TRACKER v4.93. Flower angles were measured with reference to the horizontal axis as previously described in Yon *et al.* (2016).

Auxin measurements

Complete or longitudinally halved segments were collected from plants growing under glasshouse conditions at the indicated times over a period of 1 h. Indole-3-acetic acid (IAA) was quantified as previously described (Schäfer *et al.*, 2016). Briefly, IAA was extracted from *c.* 25 mg of pooled tissue samples with 800 μl of pre-cooled (−20°C) acidified MeOH [MeOH:H_2O:HCOOH 15:4:1 (v:v:v)] containing the internal standard (3 ng d5-IAA). Samples were homogenized in a Geno/Grinder (SPEX SamplePrep) and centrifuged. Supernatants were transferred to new vials and pellets were re-extracted, following the same procedure, with 600 μl of the extraction buffer (without internal standards). Supernatants were combined and loaded into a 96-well HR-X column (Macherey-Nagel; https://www.mn-net.com). The flow-through was collected in a 96-well Nunc Deep Well Plate (Thermo Fisher; https://www.thermofisher.com) and MeOH was evaporated using a TurboVap 96 instrument (Biotage; https://www.biotage.com) at 45°C under a constant nitrogen flow. Samples were reconstituted with 850 μl 1 N HCOOH and loaded into a 96-well HR-XC column (Macherey-Nagel). Columns were washed with 1 ml 1 N HCOOH and IAA was eluted with 1 ml of acidified MeOH (0.2 N HCOOH in 80% MeOH). Samples were separated on a Bruker Advance UHPLC system equipped with a Zorbax Eclipse XDB-C18 column. IAA was analyzed using a Bruker Elite EvoQ Triple quad-MS equipped with a heated electrospray ionization (HESI) ion source. Solvent settings, source parameters and MRM-settings were previously described in Schäfer *et al.* (2016). Post-run data analysis was performed with MS DATA REVIEW software (Bruker; https://www.bruker.com).

Alternatively, IAA was quantified as previously described in Machado *et al.* (2016). Briefly, IAA was extracted from *c.* 100 mg of pooled tissue samples with 1 ml of ethyl acetate:formic acid (99.5:0.5 v/v) solution containing the internal standard (20 ng d5-IAA). Samples were vortexed for 10 min and centrifuged at 18,000 ***g*** for 20 min at 4°C. Supernatants were transferred into a new vial and evaporated under a constant nitrogen flow. Samples were reconstituted in 50 μl methanol:water (70:30) and incubated in an ultrasonic bath (Branson Ultrasonics) for 5 min. IAA was analyzed with an Agilent 1260 infinity HPLC system (Agilent; https://www.agilent.com) coupled to an API 5000 mass spectrometer (AB Sciex; https://sciex.com). Solvent settings and source parameters were as described in Machado *et al.* (2016). Post-run data analysis was performed with ANALYST 1.5 software (AB Sciex).

Pharmacological treatments

All compounds [2,3,5-triiodobenzoic acid (TIBA) (Duchefa), NPA (Duchefa), indole-3-acetic acid (IAA) (Sigma; https://www.sigmaaldrich.com) and 2,4-dichlorophenoxyacetic acid (2,4-D) (Duchefa)] were dissolved in dimethyl sulfoxide (DMSO) to make stock solutions. Lanolin mixtures were prepared by adding TIBA stock solution or DMSO to pre-warmed lanolin. For *in planta* treatments, lanolin mixtures with 1.5 mg g^{-1} of TIBA or DMSO were used for pedicel-targeted applications. Incubation solutions with 100 μM NPA, 10 μM IAA, 5 μM 2, 4-D and DMSO (1 μl ml^{-1}) were prepared in 10^{-3} M phosphate buffer pH 6.3 with 0.03% plant agar.

Real-time PCR

RNA was isolated and DNase treated with the RNeasy Plant Mini Kit (Qiagen; https://www.qiagen.com). RNA concentration was measured on a NanoDrop ND-1000 spectrophotometer and 1 μg of total RNA was subjected to reverse transcription using oligo (dT) primers (Thermo Fisher). qPCR reactions were prepared in 96-well plates (Eurogentec; https://secure.eurogentec.com) with

the Takyon master mix (Eurogentec) with Low ROX for SYBR green-based assays and the PrimeTime gene expression master mix (IDT; https://eu.idtdna.com/) for probe-based assays. Final primer concentration for SYBR green assays was 100 nM for forward and reverse primers. A primer-to-probe ratio of 2 was used for probe-based assays. Samples were processed in a Mx3005P system (Agilent). Cycling conditions for SYBR assays were one cycle of 3 min at 95°C, followed by 40 cycles of 10 sec at 95°C and 1 min at 60°C with a final cycle for post-amplification melting-curve analysis. Cycling conditions for probe-based assays were one cycle of 3 min at 95°C, followed by 40 cycles of 15 sec at 95°C and 1 min at 60°C. Data analysis was performed with the instrument software. The $2^{-\Delta\Delta CT}$ method (Livak and Schmittgen, 2001) was used for relative quantification of qPCR data.

Multiplexed gene expression analysis

Multiplexed measurement of gene expression with colour-coded probes has been described previously in Geiss *et al.* (2008). Briefly, an nCounter Elements XT assay (NanoString; https://www.nanostring.com) was used with reporter (A) and capture (B) binding probes carrying 35–50 bases of contiguous target-specific sequences (Table S1). Individual probes for each group were combined in TE buffer (10 mM Tris, 1 mM EDTA, pH 8) to create 5 and 25 nM working pools for probe A and probe B, respectively. Hybridization mix was prepared with 70 μl of hybridization buffer (NanoString), 7 μl of each probe pool and the tagset (NanoString). Hybridization was carried out at 67°C for 16 h in a thermal cycler with 8 μl of the hybridization mix and 100 ng of total RNA in a final 15 μl reaction volume. After hybridization, sample volume was adjusted to 30 μl with water and loaded into an nCounter SPRINT cartridge (NanoString). Samples were processed in the nCounter SPRINT Profiler (NanoString) and data analysis was performed using nSolver software (NanoString) as described in Khan *et al.* (2011).

Microarray analysis

Complete or longitudinally halved segments were collected from plants growing under LD at the indicated times over a period of 1 h. Total RNA from *c.* 100 mg of pooled tissue was extracted using the Plant RNeasy kit (Qiagen) and quality checked by spectrophotometry (NanoDrop; https://www.isogen-lifescience.com). Genomic DNA was removed by DNase treatment (Ambion; https://www.thermofisher.com) following the manufacturer instructions. RNA was cleaned up on RNeasy MinElute columns (Qiagen) and the RNA quality was checked using the RNA 6000 Nano kit (Agilent) in an Agilent 2100 Bioanalyzer (Agilent). RNA was labelled with cyanine-3 (Cy3) with the Quick Amp labelling kit (Agilent) according to the manufacturer's instructions, followed by RNeasy column purification (Qiagen). Dye incorporation and cRNA yield were checked with a NanoDrop ND-1000 spectrophotometer. Samples were hybridized to the *N. attenuata* whole-genome single colour array (Agilent 8× 6K, GPL19764). Slides were scanned immediately after washing using the Agilent DNA Microarray Scanner (G2565BA) with the one-colour scan setting. Probe feature extraction was performed with the feature extraction software (Agilent). Quality control, data filtering, and normalization were performed using GeneSpring GX software (Agilent). Probe signals were $\log_2$ transformed and normalized to the 75th percentile. Probe filtering was performed in GeneSpring GX using a platform flag (gIsWellAboveBG). Probes that did not pass the conditions in all replicates in at least one of the conditions were filtered out. Time-series analysis of differential expression in adaxial and abaxial pedicel tissues was performed using the Bayesian Estimation of Temporal Regulation (BETR) algorithm (Aryee *et al.*, 2009) in MultiExperiment Viewer software (MeV) (Chu *et al.*, 2008). MeV was also used for hierarchical clustering (HCL) and heatmap visualization. Differential expression analysis in pedicels of EV and *irZTL* plants at ZT0 was performed using a moderated *t*-test and with GeneSpring GX software (Agilent). Gene ontology analysis was performed using ClueGO as described in Bindea *et al.* (2009). Main GO terms were selected based on the number of associated genes in the term (Bonferroni, $P_{adj} < 0.05$). Probes to gene association and gene annotation were based on the *N. attenuata* genome assembly v2.5.

Homologous gene group identification and phylogenetic analysis

Identification of homologous gene groups and phylogenetic analysis were based on protein coding sequences from 11 eudicot species and were previously described in Brockmöller *et al.* (2017). PhyML was used to construct phylogenetic trees from the identified homologous groups and visualized using the iTOL tool (Letunic and Bork, 2007). Sequences used for the analysis are available at the *Nicotiana attenuata* data Hub (http://nadh.ice.mpg.de/NaDH/).

Tissue-specific expression analysis

Library preparation and RNA-seq data processing were previously described in Xu *et al.* (2017). Expression profiles of all predicted gene models in *N. attenuata* are provided in Xu *et al.* (2017) and are available at the *Nicotiana attenuata* data Hub (http://nadh.ice.mpg.de/NaDH/). Expression values were calculated as transcripts per million (TPM).

Subcellular localization of IAA19-like

An *A. tumefaciens* strain GV3101 harbouring 35S::IAA19-like–YFP or 35S::SV40NLS–cyan fluorescent protein (CFP) were co-infiltrated in *N. benthamiana* leaves. Two days after infiltration, confocal images of epidermal cells in the abaxial side of infiltrated leaves were acquired using a CLSM 510 confocal scanning microscope (Zeiss). Fluorescence was detected using excitation wavelengths of 458 and 514 nm and band pass filters of 475–525 nm or 530–600 nm for CFP and YFP signals. Images were processed using the LSM Image Browser (Zeiss; https://www.zeiss.com) and Photoshop 12 software (Adobe; https://www.adobe.com) was used for figure assembly.

Yeast-two-hybrid assays

The Matchmaker Gold Yeast-two-hybrid system (Clontech; https://www.takarabio.com) was used for the Y2H assay, following te manufacturer's instructions. Briefly, full-length coding sequences of *IAA19*-like and *ZTL* were amplified by PCR with gene-specific primers (data file S3) using a *Pfu* polymerase (Thermo Scientific). The resulting PCR products were cloned into the pGBKT7 or the pGADT7 vectors to generate the ZTL binding domain (BD) and the IAA19-like activation domain (AD) fused constructs. Plasmids were co-transformed into *Saccharomyces cerevisiae* strain Y2Hgold and plated in SD/−Leu/−Trp selective dropout medium. To assess protein interactions, transformed yeast was cultured in QDO (SD/−Ade/−His/−Leu/−Trp) medium with 40 mg L^{-1} of X-α-Gal. Interactions were evaluated after 3 days of incubation at 30°C.

In vitro pull-down assays

Pull-down assays were performed as described previously (Li *et al.*, 2017, 2018). His-IAA19-like fusion protein was generated

using the IAA19-like entry vector and the destination vector pDEST-N112-HIS-MBP via Gateway cloning. Glutathione *S*-transferase (GST)-tagged ZTL (GST–ZTL) was generated similarly using the destination vector pDEST15. Vectors were transformed into *Escherichia coli* BL21 (DE3) cells. Overnight bacterial cultures were transferred to 500 ml of Luria-Bertani medium containing 100 mg L^{-1} of ampicillin and grown at 37°C to an OD_{600} of 0.5. Protein expression was induced with 0.4 mM of isopropyl β-D-1-thiogalactopyranoside and cells were further grown for 3 h at 37°C or 4 h at 30°C for His-tagged and GST-tagged cultures, respectively. Proteins were purified using Ni-NTA agarose (Qiagen) for HIS-tagged and glutathione sepharose 4B (GE Healthcare; https://www.gelifesciences.com) for GST-tagged proteins according to the manufacturer's instructions. In total, 2 μg of GST, GST–ZTL or His-IAA19-like proteins were processed as described in Li *et al.* (2017) and Li *et al.* (2018). Samples and controls were subjected to SDS-PAGE and immunoblotted by anti-His antibody. Fusion proteins were visualized using Coomassie blue staining.

Co-immunoprecipitation

IAA19-like-Myc was generated using the IAA19-like entry vector and the destination vector pBA-6myc via Gateway cloning. YFP–ZTL was generated in the same way using the destination vector pEarleyGate 104. *N. benthamiana* leaves were co-infiltrated with *A. tumefaciens* GV3101 IAA19-like-Myc/YFP–ZTL or IAA19-like-Myc/YFP. Immunoprecipitation was performed as described in Li *et al.* (2017) and Li *et al.* (2018). Briefly, samples were harvested 48 h after infiltration and 5 g of tissue were used for total protein extraction in 2.5 ml lysis buffer (150 μM NaCl, 10% glycerol, 1 mM EDTA, 50 mM Tris–HCl pH 7.5, 0.5% Nonidet P-40, 2 mM DTT, 1 mM PMSF and the protease inhibitor mixture). Samples were incubated in 250 μl GFP-Trap_A beads (Chromotek) for 3 h at 4°C. Beads were washed thrice with co-immunoprecipitation buffer (150 μM NaCl, 1 mM EDTA, 50 mM Tris–HCl pH 7.5, 0.5% Nonidet P-40), re-suspended in 50 μl 2× SDS loading buffer and heated for 5 min at 95°C. Input and pulled-down samples (20 μl) were subjected to SDS-PAGE and immunoblotted using anti-Myc antibody.

ACKNOWLEDGEMENTS

We thank Matthias Schöttner, Klaus Gase, Thomas Hahn, Wibke Seibt, and Eva Rothe for technical assistance, Tamara Krügel, Andreas Weber, Andreas Schünzel and the entire glasshouse team for plant cultivation. Youngsung Joo, Wenwu Zhou, Melanie Wilson, Henrique Valim, Shree Pandey, and Jürgen Rybak for helpful discussions. This work was mostly funded by the Max Planck Society. S-GK and FY were funded by an ERC Advanced Grant no. 293926 from the European Research Council to ITB S-GK was funded by the Next-Generation BioGreen 21 Program (PJ01322603 and PJ01311601) provided by the Rural Development Administration. MS was funded by Collaborative Research Centre 'Chemical Mediators in Complex Biosystems-ChemBioSys' (SFB 1127) from the DFG to ITB. RL was funded by a Humboldt Postdoctoral Research Fellowship.

AUTHOR CONTRIBUTIONS

LCL designed the study, performed experiments, and analyzed the data. RL, FY, MS and CAMR performed experiments and analyzed the data. ITB, RH and S-GK designed and coordinated the study. LCL, and ITB wrote the manuscript.

COMPETING INTERESTS

The authors declare that they have no competing interests.

DATA AND MATERIALS AVAILABILITY

All microarray datasets were deposited in the Gene Expression Omnibus (GEO) database repository with the dataset identifiers GSE117235 and GSE116648.

SUPPORTING INFORMATION

Additional Supporting Information may be found in the online version of this article.

Figure S1. Related to Figure 1. Asymmetric transcriptional responses between adaxial and abaxial tissues of the pedicel. Violin plots showing the signal intensity of probes in clusters I, III, and V. A selection of genes associated with each cluster is shown.

Figure S2. Related to Figure 5. IAA19-like characterization. (a) Phylogenetic tree of the Aux/IAA gene family based on protein coding sequences from 11 eudicot species. The IAA5/6/19 clade is indicated in grey. Genes from different species are represented by different colours. (b) Heatmap representation of tissue-specific expression of genes of the IAA5/6/19 clade. Leaf, root, and stem treated samples were collected from WT plants treated with *Manduca sexta* oral secretions (see Brockmöller *et al.*, 2017 for additional experimental details). (c) Transcript levels of *IAA19*-like in pedicels of EV plants in response to increasing concentrations of IAA determined by hybridization with colour-coded probes (mean ± SEM, n = 3–4). Pedicels were collected at ZT0 and incubated under white light for 45 min at the indicated auxin concentration. (d) Nuclear localization of IAA19-like in epidermal cells of *N. benthamiana* leaves. From left to right: bright field, SV40NLS–CFP, IAA19-like–YFP, and merged images. Bar, 20 μm.

Figure S3. Tissue-specific and temporal expression patterns of *ZTL* in the pedicel. (a) Expression levels of *ZTL* in different tissues. Leaf, root, and stem treated samples were collected from WT plants treated with *Manduca sexta* oral secretions (see Brockmöller *et al.*, 2017 for additional experimental details). (b) Temporal expression patterns of *ZTL* and *IAA19*-like in adaxial and abaxial tissues of the pedicel.

Table S1. List of primers and probes.

Data S1. List of genes with dorsiventral expression asymmetry in pedicels of WT plants.

Data S2. Differentially expressed genes in pedicels of ir*ZTL* plants relative to the EV controls.

Movie S1. Time-lapse movie of the diurnal changes in orientation of *Nicotiana attenuata* flowers.

Movie S2. Time-lapse movie of the diurnal movement of a floral pedicel *in vitro*.

REFERENCES

Abel, S., Oeller, P.W. and Theologis, A. (1994) Early auxin-induced genes encode short-lived nuclear proteins. *Proc. Natl Acad. Sci. USA*, **91**, 326–330.

Adams, S., Manfield, I., Stockley, P. and Carré, I.A. (2015) Revised morning loops of the *Arabidopsis* Circadian clock based on analyses of direct regulatory interactions. *PLoS ONE*, **10**, 1–11.

Aryee, M.J., Gutiérrez-Pabello, J.A., Kramnik, I., Maiti, T. and Quackenbush, J. (2009) An improved empirical bayes approach to estimating differential gene expression in microarray time-course data: BETR (Bayesian Estimation of Temporal Regulation). *BMC Bioinformatics*, **10**, 409.

Atamian, H.S., Creux, N.M., Brown, E.A., Garner, A.G., Blackman, B.K. and Harmer, S.L. (2016) Circadian regulation of sunflower heliotropism, floral orientation, and pollinator visits. *Science*, **353**, 587–590.

Barlow, P.W. (1989) Differential growth in plants-A phenomenon that occurs at all levels of organization. *Environ. Exp. Bot.* **29**, 1–5.

Bindea, G., Mlecnik, B., Hackl, H., Charoentong, P., Tosolini, M., Kirilovsky, A., Fridman, W.-H., Pagès, F., Trajanoski, Z. and Galon, J. (2009) ClueGO: a Cytoscape plug-in to decipher functionally grouped gene ontology and pathway annotation networks. *Bioinformatics*, **25**, 1091–1093.

Briggs, W.R. (2014) Phototropism: some history, some puzzles, and a look ahead. *Plant Physiol.* **164**, 13–23.

Briggs, W.R., Tocher, R.D. and Wilson, J.F. (1957) Phototropic auxin redistribution in corn coleoptiles. *Science*, **126**, 210–212.

Brockmöller, T., Ling, Z., Li, D., Gaquerel, E., Baldwin, I.T. and Xu, S. (2017) *Nicotiana attenuata* Data Hub (NaDH): an integrative platform for exploring genomic, transcriptomic and metabolomic data in wild tobacco. *BMC Genom.*, **18**, 79.

Chu, V.T., Gottardo, R., Raftery, A.E., Bumgarner, R.E. and Yeung, K.Y. (2008) MeV+R: using MeV as a graphical user interface for Bioconductor applications in microarray analysis. *Genome Biol.* **9**, R118.

Covington, M.F. and Harmer, S.L. (2007) The circadian clock regulates auxin signaling and responses in *Arabidopsis*. *PLoS Biol.* **5**, 1773–1784.

Cuéllar Pérez, A. and Goossens, A. (2013) Jasmonate signalling: a copycat of auxin signalling? *Plant Cell Environ.* **36**, 2071–2084.

Darwin, C. (1880) *The Power of Movement in Plants*. London: John Murray.

Delbarre, A., Muller, P., Imhoff, V. and Guern, J. (1996) Comparison of mechanisms controlling uptake and accumulation of 2,4-dichlorophenoxy acetic acid, naphthalene-1-acetic acid, and indole-3-acetic acid in suspension-cultured tobacco cells. *Planta*, **198**, 532–541.

Dornbusch, T., Michaud, O., Xenarios, I. and Fankhauser, C. (2014) Differentially phased leaf growth and movements in *Arabidopsis* depend on coordinated circadian and light regulation. *Plant Cell*, **26**, 3911–3921.

Engelmann, W., Simon, K. and Phen, C.J. (1992) Leaf movement rhythm in *Arabidopsis thaliana*. *Zeitschrift für Naturforsch*, **47**, 925–928.

Esmon, C.A., Tinsley, A.G., Ljung, K., Sandberg, G., Hearne, L.B. and Liscum, E. (2006) A gradient of auxin and auxin-dependent transcription precedes tropic growth responses. *Proc. Natl Acad. Sci. USA*, **103**, 236–241.

Estelle, M. (1996) Plant tropisms: the ins and outs of auxin. *Curr. Biol.* **6**, 1589–1591.

Firn, R.D. and Myers, A.B. (1989) Plant movements caused by differential growth–unity or diversity of mechanisms? *Environ. Exp. Bot.* **29**, 47–55.

Geiss, G.K., Bumgarner, R.E., Birditt, B. *et al.* (2008) Direct multiplexed measurement of gene expression with color-coded probe pairs. *Nat. Biotechnol.* **26**, 317.

Haga, K. and Iino, M. (2006) Asymmetric distribution of auxin correlates with gravitropism and phototropism but not with autostraightening (autotropism) in pea epicotyls. *J. Exp. Bot.* **57**, 837–847.

Harper, R.M., Stowe-Evans, E.L., Luesse, D.R., Muto, H., Tatematsu, K., Watahiki, M.K., Yamamoto, K. and Liscum, E. (2000) The *NPH4* locus encodes the auxin response factor ARF7, a conditional regulator of differential growth in aerial Arabidopsis tissue. *Plant Cell*, **12**, 757–770.

Hatakeda, Y., Kamada, M., Goto, N., Fukaki, H., Tasaka, M., Suge, H. and Takahashi, H. (2003) Gravitropic response plays an important role in the nutational movements of the shoots of *Pharbitis nil* and *Arabidopsis thaliana*. *Physiol Plant.* **118**, 464–473.

Haverkamp, A., Li, X., Hansson, B.S., Baldwin, I.T., Knaden, M. and Yon, F. (2018) Flower movement balances pollinator needs and pollen protection. *Ecology*, **100**(1), 1–11.

Helfer, A., Nusinow, D.A., Chow, B.Y., Gehrke, A.R., Bulyk, M.L. and Kay, S.A. (2011) *LUX ARRHYTHMO* encodes a nighttime repressor of Circadian gene expression in the *Arabidopsis* core clock. *Curr. Biol.* **21**, 126–133.

Himanen, K., Boucheron, E., Vanneste, S., De Almeida, Engler J., Inzé, D. and Beeckman, T. (2002) Auxin-mediated cell cycle activation during early lateral root initiation. *Plant Cell*, **14**, 2339–2351.

Iida, M., Takano, T., Matsuura, T., Mori, I.C. and Takagi, S. (2018) Circumnutation and distribution of phytohormones in *Vigna angularis* epicotyls. *J. Plant Res.* **131**, 165–178.

Ishida, T., Adachi, S., Yoshimura, M., Shimizu, K., Umeda, M. and Sugimoto, K. (2010) Auxin modulates the transition from the mitotic cycle to the endocycle in *Arabidopsis*. *Development*, **137**, 63–71.

Jarillo, J.A., Capel, J., Tang, R.H., Yang, H.Q., Alonso, J.M., Ecker, J.R. and Cashmore, A.R. (2001) An *Arabidopsis* circadian clock component interacts with both CRY1 and phyB. *Nature*, **410**, 487–490.

Khan, M., Vaes, E. and Mombaerts, P. (2011) Regulation of the probability of mouse odorant receptor gene choice. *Cell*, **147**, 907–921.

Kiba, T., Henriques, R., Sakakibara, H. and Chua, N.-H. (2007) Targeted degradation of PSEUDO-RESPONSE REGULATOR5 by an SCF^{ZTL} complex regulates clock function and photomorphogenesis in *Arabidopsis thaliana*. *Plant Cell*, **19**, 2516–2530.

Kim, W.-Y., Fujiwara, S., Suh, S.-S., Kim, J., Kim, Y., Han, L., David, K., Putterill, J., Nam, H.G. and Somers, D.E. (2007) ZEITLUPE is a circadian photoreceptor stabilized by GIGANTEA in blue light. *Nature*, **449**, 356–360.

Krügel, T., Lim, M., Gase, K., Halitschke, R. and Baldwin, I.T. (2002) *Agrobacterium*-mediated transformation of *Nicotiana attenuata*, a model ecological expression system. *Chemoecology*, **12**, 177–183.

Kutschera, U. and Schopfer, P. (1986) Effect of auxin and abscisic acid on cell wall extensibility in maize coleoptiles. *Planta*, **167**, 527–535.

Letunic, I. and Bork, P. (2007) Interactive Tree Of Life (iTOL): an online tool for phylogenetic tree display and annotation. *Bioinformatics*, **23**, 127–128.

Li, Y., Hagen, G. and Guilfoyle, T.J. (1991) An auxin-responsive promoter is differentially induced by auxin gradients during tropisms. *Plant Cell*, **3**, 1167–1175.

Li, R., Wang, M., Wang, Y., Schuman, M.C., Weinhold, A., Schäfer, M., Jiménez-Alemán, G.H., Barthel, A. and Baldwin, I.T. (2017) Flower-specific jasmonate signaling regulates constitutive floral defenses in wild tobacco. *Proc. Natl Acad. Sci. USA*, **114**, E7205–E7214.

Li, R., Cortés Llorca, L., Schuman, M.C., Wang, Y., Wang, L., Joo, Y., Wang, M., Vassão, D.G. and Baldwin, I.T. (2018) ZEITLUPE in the roots of wild tobacco regulates jasmonate-mediated nicotine biosynthesis and resistance to a generalist herbivore. *Plant Physiol.* **177**, 833–846.

Liu, H., Wang, Q., Liu, Y., Zhao, X., Imaizumi, T., Somers, D.E., Tobin, E.M. and Lin, C. (2013) *Arabidopsis* CRY2 and ZTL mediate blue-light regulation of the transcription factor CIB1 by distinct mechanisms. *Proc. Natl Acad. Sci. USA*, **110**, 17582–17587.

Livak, K.J. and Schmittgen, T.D. (2001) Analysis of relative gene expression data using real-time quantitative PCR and the $2^{-\Delta\Delta CT}$ method. *Methods*, **25**, 402–408.

Löfke, C., Zwiewka, M., Heilmann, I., Van Montagu, MCE, Teichmann, T. and Friml, J. (2013) Asymmetric gibberellin signaling regulates vacuolar trafficking of PIN auxin transporters during root gravitropism. *Proc. Natl Acad. Sci. USA*, **110**, 3627–3632.

Machado, R.A.R., Robert, C.A.M., Arce, C.C.M., Ferrieri, A.P., Xu, S., Jimenez-Aleman, G.H., Baldwin, I.T. and Erb, M. (2016) auxin is rapidly induced by herbivore attack and regulates a subset of systemic, jasmonate-dependent defenses. *Plant Physiol.* **172**, 521–532.

de Mairan, J.-J. (1729) Observation botanique. Hist l'Académie R des Sci avec les mémoires mathématique Phys tirés des Regist cette Académie, 35–36.

Más, P., Kim, W.-Y., Somers, D.E. and Kay, S.A. (2003) Targeted degradation of TOC1 by ZTL modulates circadian function in *Arabidopsis thaliana*. *Nature*, **426**, 567–570.

Millar, A.J., Carre, I.A., Strayer, C.A., Chua, N.H. and Kay, S.A. (1995) Circadian clock mutants in *Arabidopsis* identified by luciferase imaging. *Science*, **267**, 1161–1163.

Morris, D.A., Friml, J. and Zažímalová, E. (2010) The transport of auxins. In *Plant Horm. Biosynthesis, Signal Transduction, Action!* (Davies, P. J. ed.). Dordrecht: Springer Netherlands, pp. 451–484.

Nakamichi, N., Kiba, T., Henriques, R., Mizuno, T., Chua, N.H. and Sakakibara, H. (2010) PSEUDO-RESPONSE REGULATORS 9, 7, and 5 are transcriptional repressors in the *Arabidopsis* circadian clock. *Plant Cell*, **22**, 594–605.

Niinuma, K., Someya, N., Kimura, M., Yamaguchi, I. and Hamamoto, H. (2005) Circadian rhythm of circumnutation in inflorescence stems of *Arabidopsis*. *Plant Cell Physiol.* **46**, 1423–1427.

Nishitani, K. and Masuda, Y. (1981) Auxin-induced changes in the cell wall structure: changes in the sugar compositions, intrinsic viscosity and molecular weight distributions of matrix polysaccharides of the epicotyl cell wall of *Vigna angularis*. *Physiol. Plant*, **52**, 482–494.

Paponov, I.A., Paponov, M., Teale, W., Menges, M., Chakrabortee, S., Murray, J.A.H. and Palme, K. (2008) comprehensive transcriptome analysis of auxin responses in *Arabidopsis*. *Mol. Plant*, **1**, 321–337.

Phillips, I.D.J. (1972) Endogenous gibberellin transport and biosynthesis in relation to geotropic induction of excised sunflower shoot-tips. *Planta*, **105**, 234–244.

Rawat, R., Schwartz, J., Jones, M.A., Sairanen, I., Cheng, Y., Andersson, C.R., Zhao, Y., Ljung, K. and Harmer, S.L. (2009) REVEILLE1, a Myb-like transcription factor, integrates the circadian clock and auxin pathways. *Proc. Natl Acad. Sci. USA*, **106**, 16883–16888.

Rayle, D.L., Evans, M.L. and Hertel, R. (1970) Action of auxin on cell elongation. *Proc. Natl Acad. Sci. USA*, **65**, 184–191.

Roudier, F., Fedorova, E., Lebris, M., Lecomte, P., Györgyey, J., Vaubert, D., Horvath, G., Abad, P., Kondorosi, A. and Kondorosi, E. (2003) The Medicago species A2-type cyclin is auxin regulated and involved in meristem formation but dispensable for endoreduplication-associated developmental programs. *Plant Physiol.* **131**, 1091–1103.

Ruan, C.-J. and da Silva, J.A.T. (2011) Adaptive significance of floral movement. *CRC Crit. Rev. Plant Sci.* **30**, 293–328.

Saitoh, A., Takase, T., Kitaki, H., Miyazaki, Y. and Kiyosue, T. (2015a) Gene expression profile of *zeitlupe/lov kelch protein1* T-DNA insertion mutants in *Arabidopsis thaliana*: downregulation of auxin-inducible genes in hypocotyls. *Plant Signal. Behav.* **10**, e1071752.

Saitoh, A., Takase, T., Kitaki, H. and Kiyosue, T. (2015b) Gene expression profile of *Arabidopsis* plants that overexpress ZEITLUPE/LOV KELCH PROTEIN1: up-regulation of auxin-inducible genes in hypocotyls. *Plant Biotechnol.* **32**, 257–261.

Sato, A., Sasaki, S., Matsuzaki, J. and Yamamoto, K.T. (2014) Light-dependent gravitropism and negative phototropism of inflorescence stems in a dominant Aux/IAA mutant of *Arabidopsis thaliana*, *axr2*. *J. Plant Res.* **127**, 627–639.

Schäfer, M., Brütting, C., Baldwin, I.T. and Kallenbach, M. (2016) High-throughput quantification of more than 100 primary- and secondary-metabolites, and phytohormones by a single solid-phase extraction based sample preparation with analysis by UHPLC–HESI–MS/MS. *Plant Methods*, **12**, 30.

Schneider, C.A., Rasband, W.S. and Eliceiri, K.W. (2012) NIH Image to ImageJ: 25 years of image analysis. *Nat. Methods*, **9**, 671.

Schuman, M.C., Palmer-Young, E.C., Schmidt, A., Gershenzon, J. and Baldwin, I.T. (2014) Ectopic terpene synthase expression enhances sesquiterpene emission in *Nicotiana attenuata* without altering defense or development of transgenic plants or neighbors. *Plant Physiol.* **166**, 779–797.

Shalit-Kaneh, A., Kumimoto, R.W., Filkov, V. and Harmer, S.L. (2018) Multiple feedback loops of the *Arabidopsis* circadian clock provide rhythmic robustness across environmental conditions. *Proc. Natl Acad. Sci. USA*, **115**, 7147–7152.

Somers, D.E., Schultz, T.F., Milnamow, M. and Kay, S.A. (2000) *ZEITLUPE* encodes a novel clock-associated PAS protein from *Arabidopsis*. *Cell*, **101**, 319–329.

Staswick, P.E., Serban, B., Rowe, M., Tiryaki, I., Maldonado, M.T., Maldonado, M.C. and Suza, W. (2005) Characterization of an Arabidopsis enzyme family that conjugates amino acids to indole-3-acetic acid. *Plant Cell*, **17**, 616–627.

Taniguchi, M., Nakamura, M., Tasaka, M. and Morita, M.T. (2014) Identification of gravitropic response indicator genes in *Arabidopsis* inflorescence stems. *Plant Signal. Behav.* **9**, e29570.

Tatematsu, K., Kumagai, S., Muto, H., Sato, A., Watahiki, M.K., Harper, R.M. and Yamamoto, K.T. (2004) *MASSUGU2* encodes Aux/IAA19, an auxin-regulated protein that functions together with the transcriptional activator NPH4/ARF7 to regulate differential growth. *Plant Cell*, **16**, 379–393.

Tong, Meixuezi, Lee, Kyounghee, Ezer, Daphne *et al.* (2020) The evening complex establishes repressive chromatin domains via H2A.Z deposition. *Plant Physiol.* **182**, 612–625.

Vinterhalter, D., Vinterhalter, B., Miljuš-Djukić, J., Jovanović, Ž. and Orbović, V. (2014) Daily changes in the competence for photo- and gravitropic response by potato plantlets. *J. Plant Growth Regul.* **33**, 539–550.

Went, F.W. (1928) Wuchsstoff und Wachstum. *Rec. Trav. Bot. Neerl.* **25**, 1–116.

Wright, M., Osborne, D.J. and Mousdale, D.M.A. (1978) Evidence for a gravity-regulated level of endogenous auxin controlling cell elongation and ethylene production during geotropic bending in grass nodes. *Biochem. und Physiol. der Pflanz.* **172**, 581–596.

Xu, S., Brockmöller, T., Navarro-Quezada, A. *et al.* (2017) Wild tobacco genomes reveal the evolution of nicotine biosynthesis. *Proc. Natl Acad. Sci. USA*, **114**, 6133–6138.

Yon, F., Joo, Y., Cortés Llorca, L., Rothe, E., Baldwin, I.T. and Kim, S.G. (2016) Silencing *Nicotiana attenuata LHY* and *ZTL* alters circadian rhythms in flowers. *New Phytol.* **209**, 1058–1066.

Yon, F., Kessler, D., Joo, Y., Cortés Llorca, L., Kim, S.G. and Baldwin, I.T. (2017) Fitness consequences of altering floral circadian oscillations for *Nicotiana attenuata*. *J. Integr. Plant Biol.* **59**, 180–189.